Chapter 9. Smart Energy Management and Conversion

Mike Hayes, James F. Rohan, Wensi Wang, Ningning Wang, Aldo Romani, Enrico Macrelli, Michele Dini, Matteo Filippi, Marco Tartagni, Denis Flandre

11.1 Introduction

In the past few years, wireless sensor networks (WSN) have emerged from the research domain to providing commercial solutions for many real-world applications. Currently, several WSN solutions have already been deployed in volume in commercial applications [1]. Among the anticipated applications, one of the areas of greatest potential is in Building Energy Management (BEM). By monitoring artificial lighting, temperature, carbon dioxide level, relative humidity, positioning of external shading devices and resultant actuation, a considerable percentage of energy can be saved and human comfort levels can be improved. For example, about 35% of North America's energy usage [2] and over 37% of CO_2 emissions [3] are attributed to the running of residential and commercial buildings. It has been estimated that the usage of intelligent sensor networks can result in 15-20% savings in total energy usage [4]. Due to such potential financial benefits and the political 'green agenda', intensive research interests have been focused on this area [5].

Ease of deployment may enable these radio frequency based sensor systems to replace most of the current 'wired' (cable-connected) sensor systems in the foreseeable future. However, one major bottleneck for all WSN deployments has yet to be solved. This problem is the limited system lifetime due to the insufficient energy capacity of the small form factor battery power supply. For example, a wireless sensor node designed at the Tyndall National Institute with temperature and relative humidity sensors [6] consumes an average of 0.25 mW when it operates on a low 0.1% duty cycle (fraction of time when sensing and transmitting occurs). Theoretically, powering from two standard 2000 mAh AA battery cells requires battery replacement approximately every 200 days. In practice, however, the battery life time is even shorter due to leakage currents, temperature fluctuations, environmental humidity and other variable factors [7]. With the increasing deployment scale of nodes in WSN systems, for commercial, technical and logistical reasons, the market demands a 'deploy and forget' solution requiring the elimination of a battery replacement maintenance cycle. Energy harvesting technology could lead to this possibility of self-sustaining "infinite" lifetime motes, or at least the prolongation on the life span between battery replacements. This is becoming a significant focus area in WSN research in recent years because of the necessity of bridging the gap between the continuous power consumption of the WSN mote and the limited available energy from the battery technology [8].

Many types of ambient energy sources are available. However, light illuminance [9], temperature gradients [10] and vibrations [11] have drawn the most attention within the research community, as a result of their relatively high technology readiness levels. For example, Table I shows the power density which has been obtained from different energy harvesting sources potentially available in BEM applications, i.e. indoor office illuminance, outdoor illuminance, human and machine vibration energy, building thermal energy.

Table I. Power density of various energy harvesting technologies

Energy sources	**Power density**
Indoor light (office 500lux) [9]	300μW/cm^2
Outdoor light (Standard, AM1.5)	100mW/cm^2
Shoe Insert Piezoelectric [12]	300μW/cm^3
Mechanical vibration [13]	45μW/cm^3
Thermoelectric (10^{o}C gradient) [14]	15μW/cm^3

In this chapter, the power management circuits for indoor light energy harvesting, thermoelectric energy harvesting and vibration energy harvesting are introduced. The objective of power management circuit design is towards higher conversion efficiency, ultra-low power consumption and low energy storage leakage losses.

11.2. Power management solutions for energy harvesting devices

This section focuses on the design of power management circuits for energy harvesting technologies. The concept, design and implementations are introduced in detail. For thermoelectric energy harvesting, the main challenge is due to the ultra-low voltage of the thermoelectric generator (TEG) module. Ultra-low voltage DC-DC converters are designed for this application. For photovoltaic energy harvesting, particularly indoor solar, the main challenge is low power maximum power point tracking (MPPT) design. For vibration energy harvesting, the main difficulty is high efficiency AC-DC conversion. In addition to the power management circuits, the energy storage unit is also an essential part of the system to store the energy and deliver the energy to the load.

11.2.1 Ultra-low Voltage Thermoelectric Energy Harvesting

Thermoelectric generators usually provide output voltages as low as tens of mV/K, with very low electrical series resistances [15]. Although thermoelectric generators with output voltages in the range of hundreds of mV/K based on microelectronic technologies are available [16], such devices also present high electrical resistances in the order of hundreds of Ω. For this reason, energy harvesting from thermal gradients generally requires handling very low input voltages, well below the threshold voltages of diodes or transistors, which prevent the use of conventional charge pumps or switching converters in order to boost the available voltage. This is essential for implementing fully autonomous and battery-less solutions, in which activating application circuits from a fully discharged state is mandatory.

When the input voltages are lower, but still comparable in their order of magnitude to the threshold voltages of diodes and transistors, integrated circuit technology still enables design of charge pumps operating in a sub-threshold region, such as for example in [17]. Other techniques, such as Vth-programming, as in [18], allow further reductions of the minimum activation voltage down to about 100 mV, at the expense of additional fabrication steps. In general, the minimum requirement for the input voltage is the activation of an oscillator circuit, which then drives a capacitive charge pump or a switching converter. For this reason, threshold voltages of devices play an important role.

However, with input voltage in the order of tens of mV, other types of solutions are necessary. For example, in [19] a boost converter is used in order to pump up the voltage, but the switches initially require a mechanical activation for transferring energy from the thermoelectric transducer to an inductor. This overcomes the problem of handling voltages much lower than the threshold voltage. However, a suitable mechanical excitation is not generally available in all types of solutions.

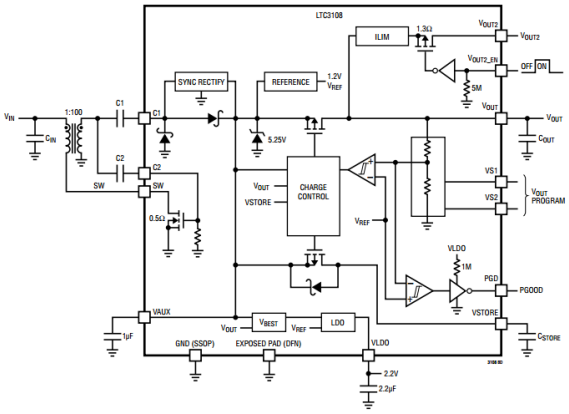

Fig. 1. Block diagram of the Linear Technology LTC3108 [21]

A suitable approach for boosting very low voltages with no external energy source is the use of transformers. Such devices can be used to build up oscillators based on the Armstrong or the Meissner topologies, in which the feedback is generated by means of magnetically coupled inductors. When very low voltages are involved, in this type of solution a normally-on transistor, such as a depletion mode MOSFET or a JFET is usually required, in order to achieve a sufficient transconductance. This type of solutions has been proposed since some time ago [20]. Recently, a very popular integrated circuit has also been developed by Linear Technologies [21] and adopts a similar topology. The LTC3108, shown in Fig. 1, implements the above mentioned oscillator topology, and is reported to operate with input voltages as low as 20 mV. The IC also implements a complete power management system. However, the IC requires an external transformer with turn ratios of some tens to one, depending on the amplitude of the input voltage. This device allows current to flow from the thermoelectric generator through the primary winding of the transformers, despite the very low input voltages. The excitation that propagates to the secondary winding of the transformer generates a feedback on the transistor, usually on the gate terminal, which modulates the primary current. An oscillation is then started, and the higher number of turns on the secondary winding generates a higher voltage. At this point, a diode rectifier or even a passive voltage multiplier can be used to collect electrical charge at voltages much higher than the input. An extension of this topology was also presented in [22], in which after the start-up, the transformer is re-used in a more conventional switching converter, in order to improve efficiency during steady-state operation, once the circuit is started.

In this perspective, it is essential to shrink the dimension of the magnetic components in order to achieve even higher levels of integration. In-package and on-chip integration are expected to bring significant advantages. In this context, the main problem is to achieve sufficient performance and to guarantee minimum losses, both in the magnetic core and in the electrical conductors. The Nanofunction project has investigated this problem and elaborated a series of solutions. The research activity involved modeling and fabrication of new topologies of integrated micro-transformers, which are to be merged in a startup oscillator integrated circuit for an ultra-low voltage harvesting solution. New topologies of micro-transformers which use bonding wires and patterned magnetic core, so called bondwire transformers [23], have been designed and modeled. Since the startup converter requires high self-inductance and turns ratio to reach and maintain the oscillation, several types of magnetic cores to be mounted on-top of the micro-transformers have been investigated. Various high permeability and high saturation commercial cores are chosen and collected such as LTCC magnetic tapes, ferrite toroids and thin-films. Moreover, various core shapes and thicknesses are selected and cut to minimize the footprint area of the prototypes. Since the startup converter requires low DC series resistance, various bonding wires have been modeled in terms of material, dimension and pad pitch. Bondwire transformer prototypes have also been realized on a PCB substrate with an ultra-thin and ultra-narrow technology.

In the design of a power micro-magnetic components such as micro-inductors and micro-transformers the choice of the magnetic structure is crucial in order to achieve high-inductance, minimize resistive losses at high frequency, and carry out the largest current available without saturating the core. The structure of micro-magnetic devices can be categorized into two main approaches which depend on the arrangements between coils and core. In the first one the planar coils are enclosed by a multilevel magnetic core (such as spiral inductors), while in the second one the multilevel conductors are wrapped around a planar magnetic core (such as toroidal and bondwire inductors). Generally, the main factors which characterize a good power micro-inductor are high inductance value per unit area, low dc resistance to get high current, high Q-factor to maximize efficiency, and miniaturization capability which can be referred as Power Supply in Package (PwrSiP) and Power Supply on Chip (PwrSoC) [24].

Table II. Summary of integrated soft magnetic materials used for power micro-magnetic components

Frequency	**Material**	**Deposition**	**Good**	**Bad**
Low frequency (fop <1 MHz)	Soft ferrites (NiZn, MnZn)	Screen printing (IC not compatible)	↑ ρc, ↑ tc	↓ Bs, ↓ μrc, ↑ Hc
High frequency (fop >5 MHz)	Metallic thin films (NiFe, NiFeMo)	Sputtering, Electroplating (IC compatible)	↑ Bs, ↓ Hc, ↑ μrc,	↓ ρc, ↓ tc
Very high frequency (fop >100 MHz)	Laminated metallic thin films nanocomposites	Sputtering, Electroplating (IC compatible)	↑ Bs, ↓ Hc,	↓ ρc,↓ tc

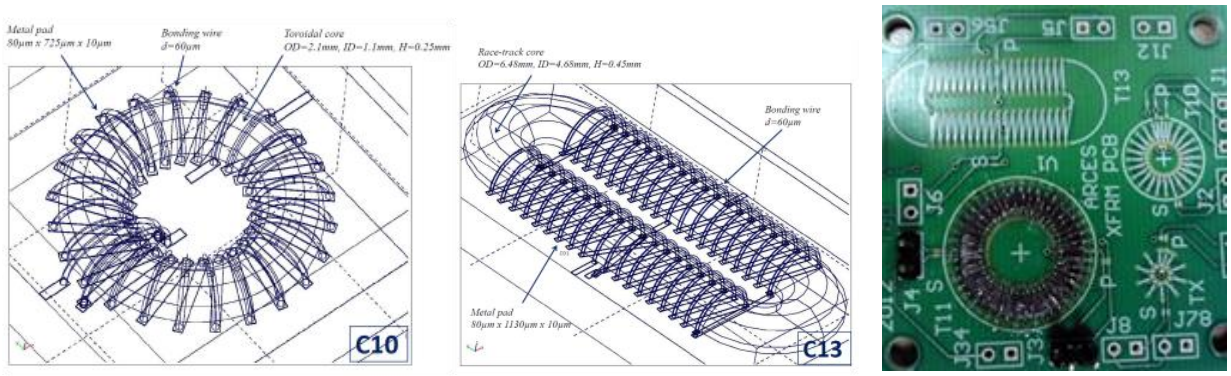

Fig. 2. Prototypes of bonding-wire transformers developed in the Nanofunction project. Toroidal (left) and race-track (centre) topologies have been developed, and tested on a PCB prototype (right)

The choice of the magnetic material is also shown to be essential. The main characteristics which define the performance of soft magnetic materials are: high resistivity, low coercivity, high saturation flux density, high relative permeability, high anisotropy field, and low core losses. High resistivity ρc [Ω·m] leads low eddy current effects in the core which represents a dissipative loss of energy within the core and define the maximum operation frequency fop [Hz]. Furthermore, a high resistivity material has an increased skin depth δc [m] which ensures that the magnetic field intensity is constant with the film thickness tc [m]. Low coercivity Hc [Oe] minimizes hysteresis loss at high frequencies, while high saturation flux density Bs [T] enhances current-handling capability. In order to get stable performance the core should have high relative permeability μrc constant for high frequencies, and high anisotropy field Hk which increases the operation frequency and current-handling ability. The core losses are mainly composed of two different contributions: eddy current losses and hysteresis losses. Low core losses require soft magnetic materials with high resistivity and low coercivity field. Table II shows a summary of integrated soft magnetic materials used for power devices.

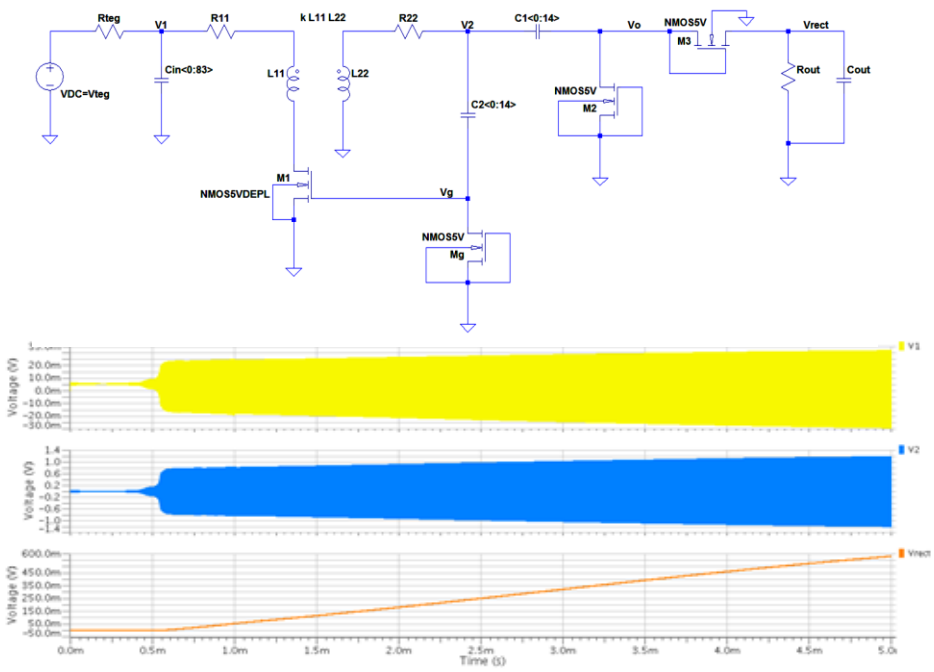

Fig. 3. Main oscillator topology with output rectifier (top). Circuit simulations of proposed converter and bonding wire transformer with n=36.5. Steady-state response of primary voltage V1 (top graph), secondary voltage V2 (middle graph), and rectified output voltage Vrect (bottom graph) with Vteg=40 mV, Rteg=430 mΩ, Cout=10 nF, Rout=100 MΩ, single M1 and two parallel C1.

Among the developed prototypes interesting results have been found. A toroidal transformer with a 4.95×4.95 mm^2 surface area enables turn ratios up to 1:38 when using gold conductors 80 µm wide. Fig. 2 shows preliminary prototypes, based on two types of geometries. All the developed technologies, besides PCB implementations, are suitable for on-chip or in-package assembly. In order to validate system design, an integrated circuit implementing the schematic reported in Fig. 3 was designed and fabricated. The proposed integrated circuit, suitable for operation with the above bondwire transformers, is based on a Meissner oscillator topology, as explained previously. Simulation results show that the proposed integrated solution, based on a CMOS integrated circuit and on the proposed micro-transformer, ensures circuit start-up and a sufficient output voltage allowing above threshold operation of a conventional boost converter. The solution is compatible with on-chip or in-package assembly and is expected to provide performance comparable to external miniaturized magnetic components, thus yielding to a higher level of integration in electronic design.

11.2.2 Sub-1mW Photovoltaic Energy Harvesting

High accuracy MPPT circuits for large scale PV cells often consume over 100 mW of power, several orders of magnitude higher than the harvested power in the small PV cell, obviously not suitable for this application [25]. Several methods have been proposed to perform low power MPPT. Simjee and Chou proposed a PFM controller based fractional open circuit voltage (FVOC) MPPT method utilizing a buck converter structure. This MPPT operates above 80% at 20mW solar power [26]. Dondi et al introduce a PWM controller based FVOC MPPT with a similar buck converter structure and achieve up to 85% efficiency when PV cell generates 50mW [27]. In [28], Brunelli suggests that it is possible to obtain MPPT power consumption around 1mW with the FVOC MPPT method with optimized frequency and components selection. These work, although significantly enhancing the MPPT performance in lower power conditions, but still exceed the sub-mW PV cell output power. Brunelli

suggests that due to the power consumption in the MPPT, for a small solar cell is impractical to use the MPPT to improve conversion efficiency, and alternative methods should be adopted [29]. Tan and Panda proposed a MPPT solution for wind energy harvesting using boost converter structure to perform impedance matching through resistance emulator method [30]. This method shows the potential to further reduce the power consumption of MPPT theoretically into sub-mW scale by adopting a low duty cycle ultra-low power microcontroller but was not verified by Tan and Panda due to difference in applications. Both [26] and [30] need a microcontroller to generate MPPT control signal, which obviously increases the system cost and complexity. Chini introduced a PFM controlled boost converter similar to the design shown in this work with components selection for ultra-low power level, however, without synchronous rectification MPPT [31].

Table III. Comparison of MPPT efficiency in lowest useable power level

	Chini et. Al [31]	Simjee et. al [26]	Tan et. al [30]	Simjee et. al [32]	Dondi et. al [27]
Converter	Boost	Buck	Boost	Buck	Buck
Control Logic	PFM Control	PFM Control	PWM Control	PFM Control	PWM Control
Input Power	1.6mW	5mW	9.36mW	10mW	50mW
Efficiency	30%	47%	84%	45%	85%

Table III. shows a comparison of efficiency among various maximum power point tracking circuits at various power levels. A system architecture of the indoor PV cell powered WSN is presented in Fig 4. This proposed power autonomous system consists of five building blocks: i) photovoltaic cells; ii) MPPT tracker; iii) energy storage units; iv) output stage voltage regulator; v) wireless sensor node. By adopting this system architecture, both the input power and output power are optimized to ensure delivery of the maximum amount of useable energy to the wireless sensor node. The multiple stage regulation reduces the energy conversion efficiency, a trade-off exists in the power losses and power gains in the power regulations. The main power losses in the system are illustrated in Fig. 5. The power (voltage) level of the energy storage unit is monitored by the wireless sensor node in order to update the network on the remaining energy in each module. The power monitoring readings and power management simulations can provide an effective means to predict the system operation.

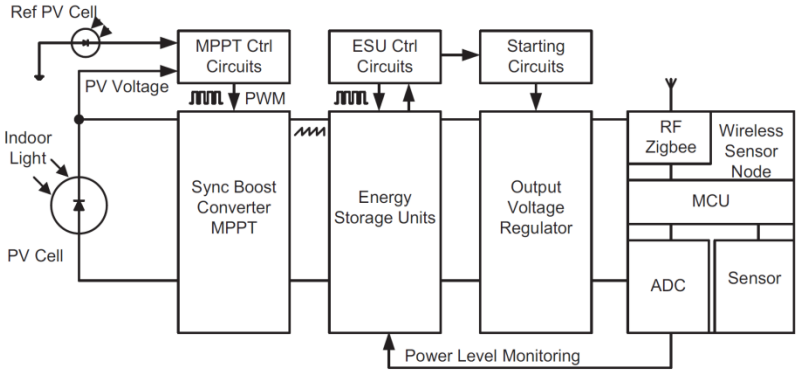

Fig. 4. Indoor light energy harvesting wireless sensor node

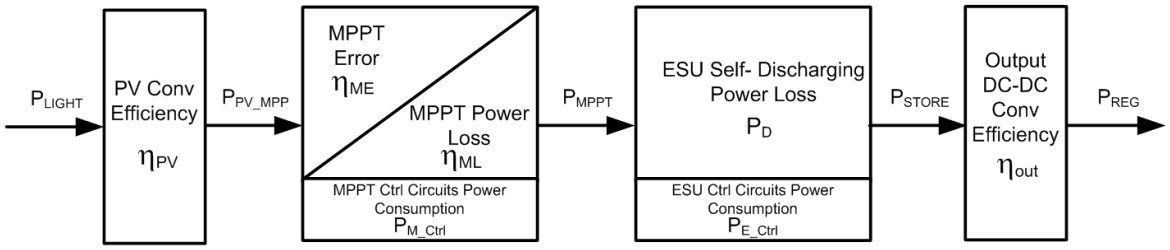

Fig. 5. Efficiency losses and power consumptions in the proposed energy harvester

The indoor light power P_{Light} is harvested by the COTS amorphous silicon photovoltaic cell with a conversion efficiency at η_{PV}. The MPPT circuits adjust the control signal frequency based on lighting intensity to approach a near optimal voltage on the PV cell, thus approaching the ideal maximum power of PV cell P_{PV_MPP}.

A certain amount of power is lost due to the imprecision of MPPT, the efficiency loss due to the MPPT error is η_{ME} as shown in Fig. 5. Inevitable efficiency losses in the MPPT procedure and the power consumption of the MPPT control circuits are expressed as η_{ML} and P_{M_Ctrl}. The output power of MPPT is expressed as P_{MPPT}. Based on input voltage and remaining energy in the ESU (energy storage unit), the ESU control circuits choose to charge/discharge the hybrid energy storage. In both charging and discharge processes, a self-discharge power loss exists as P_D. Similarly to the MPPT control circuit's power consumption, the ESU control circuit also has a power consumption P_{E_Ctrl}. The power transferred from ESU P_{STORE} is further optimized in the output voltage regulator, with an efficiency η_{out}, before connecting to the wireless sensor node. The boost converter based output voltage regulator can be automatically started up by the ESU control circuits in case of power failure and the subsequent need to restart the system.

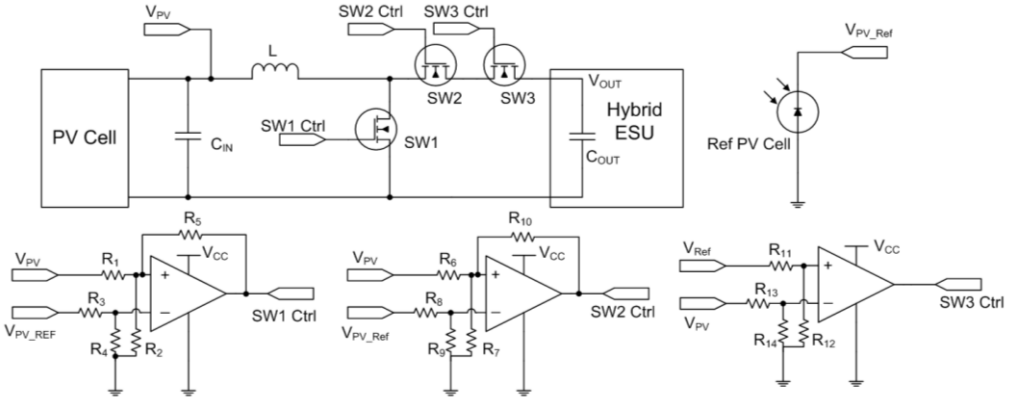

Fig 6. Conceptual Schematics of Maximum Power Point Tracking

The schematic of the synchronous boost converter based MPPT is shown in Fig 6. The MPPT consists of two main building blocks. 1) Comparator based MPPT controller 2) synchronous boost converter. The boost converter is controlled by PWM signals generated from the ultra-low power comparators. A secondary PV cell is used to obtain a reference open circuit voltage to set the theoretical V_{MPP}. Made from the same photovoltaic technology of the main PV cell, the pilot PV cell obtains an open circuit voltage V_{oc_ref} proportional to the main PV cell open circuit voltage. Hysteresis is adopted in the design to switch on transistor SW1 when input capacitor voltage (PV cell voltage) is higher than $V_{MPP}+V_{hyst1}$. The input capacitor is then discharged whilst the inductor L is charged with variable current iL(t). Once the capacitor voltage drops to VMPP -Vhyst1, the SW1 is turned off due to the hysteresis, the "ON" state time is t0~t1 as shown in Fig. 7.

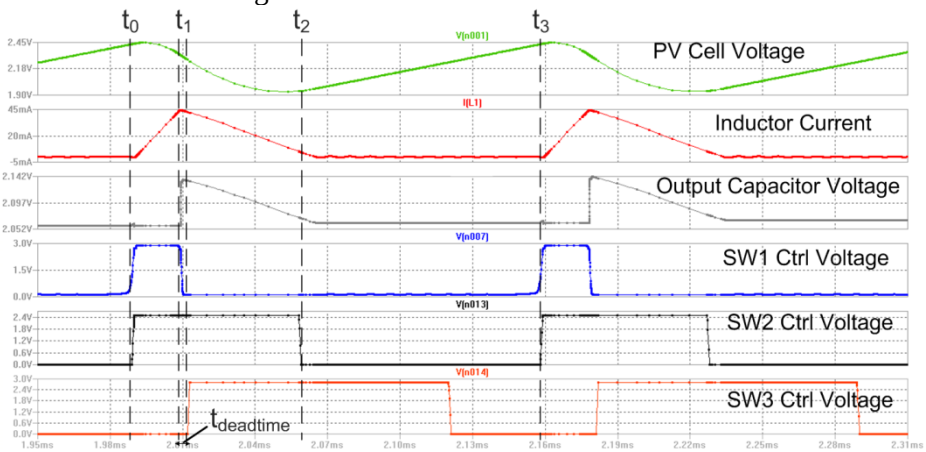

Fig. 7. Converter simulation and control signals of SW1, SW2 and SW3

The average V_{mppt} is at 0.773 of the measured open circuit voltage. The average MPPT error is less than 1.8% of the ideal MPP ratio 0.760. The employment of the MPPT circuits achieves a 27% power increase when 500 lux illuminance is applied. It can be concluded that with an ultra-low power design of the maximum power point tracker, the MPPT can improve the power conversion efficiency. However, a considerable percentage of power loss is attributed to the MPP tracker. For low illuminance light energy harvesting, the power loss offsets most of the power gained from MPPT. The ultra-low current consumption of the MPPT subsystem enables the prototype increase the power harvested from the PV cells by 30% in a 500 lux lighting condition. The carefully simulated and successfully implemented design consumes less than 50 μW power. The conversion efficiency with 0.5mW input power is 81%.

11.2.3 Piezoelectric and Micro-electromagnetic Energy Harvesting

Vibrations are widely diffused and common in several environments, for example, to name a few, humans and goods transportation or industrial machinery. Piezoelectric transducers can achieve high power density [33] and several techniques [34-37] have been developed in the past years to improve the effectiveness of the energy extraction process.

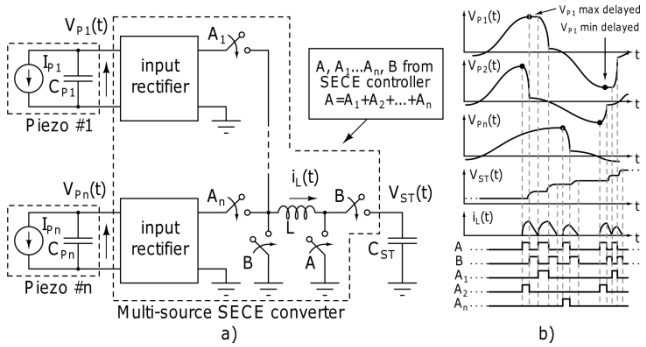

Fig. 8. (a) block diagram of a multi-source SECE converter for piezoelectric transducers, (b) qualitative waveforms under ideal conditions[39].

Converters based on synchronous electrical charge extraction (SECE) scheme (Fig.8.a) have proven to be more efficient than other passive interfaces (e.g. diode full bridge) and enable extraction of energy without any constraint between input voltage $V_P(t)$ and output voltage $V_{ST}(t)$. Moreover, harvesting energy from multiple piezoelectric transducers is a viable solution in order to increase input power [38]: each extraction cycle lasts a small fraction of the repetition period (i.e. the vibration frequency) so a single shared inductor can be exploited to extract energy from several transducers (Fig. 8.b). Simultaneous requests to access the shared inductor can be handled delaying all the requests but one.

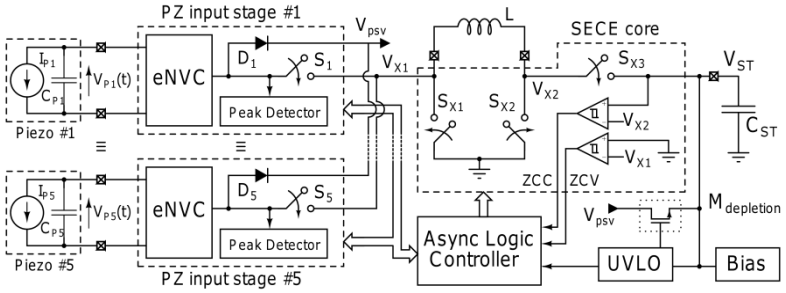

Fig. 9. Top-level schematic of a multi-source converter for energy harvesting from independent piezoelectric transducers [7].

Fig. 9. shows the top-level schematic of a multi-source converter suitable for piezoelectric energy harvesting [39]. Each transducer is connected to its input stage which rectifies the input voltage $V_{P1...5}(t)$ throughout an enhanced version of a Negative Voltage Converter (eNVC, Fig. 10.a) and then detects, with a peak detector, when the transducer voltage has reached a maximum, in order to trigger the start of an energy extraction cycle. The eNVC output is a rectified version of input voltage without forcing a way for current flow. Furthermore the n-channel MOSFETs MA1-MB2 allows the complete discharge of CP, thus an increment of available energy for each energy extraction. Important features for an energy harvesting converter are the energetic autonomy and capability to start to operate from a no-energy state (i.e. V_{ST}=0 V): a passive path (D1-D5 and Mdepletion in Fig. 9. has been implemented to allow self-start-up. Such a path is then disabled when the output voltage reaches a minimum level to guarantee correct operations of all circuits (V_{ST}>1.4 V). The logic controller has been designed with asynchronous logic in order to avoid energy waste due to clock generation and manages the issues related to inductor sharing. In addition, the logic controller determines the correct timing for each conversion phase, based on the information provided by the voltage and current zero crossing circuits (ZCV and ZCC, respectively) included in the SECE core (Fig. 9). Moreover, the SECE core embodies the power MOSFETs and their gate drivers together with a dynamic biasing circuit to further reduce the quiescent current drawn by the circuit.

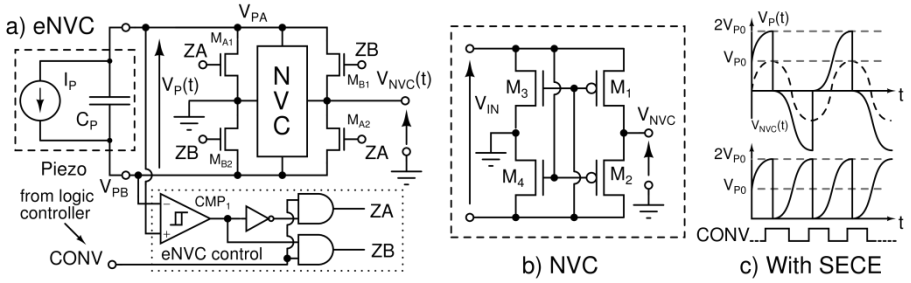

Fig. 10. (a) eNVC and its driver circuit, (b) standard NVC, (c) qualitative waveforms of input, output and control signal of the eNVC [39].

The nano-power IC [39] designed for energy harvesting from multiple independent piezoelectric transducers reaches an efficiency that ranges from 70% to over 85%, including its own power consumption.

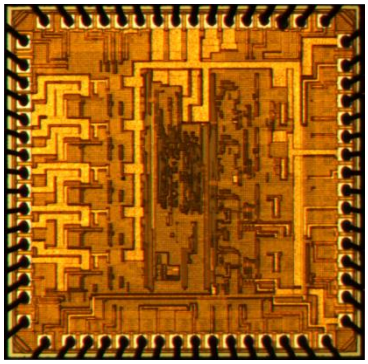

Fig. 11. Die photograph of the designed IC.

Thanks to nano-power design and energy aware techniques, the converter consumes a very low energy both during the extraction process and in the time between extractions. The quiescent power is as low as 175 nW per source at VST=2.5 V, leading to an overall quiescent power of 875 nW for handling five piezoelectric transducers. The IC, manufactured in a 0.32 μm BCD technology, has an area of 4.6 mm^2 and the die photograph is shown in Fig. 11.

11.2.4 DC/DC Power Management for Future Micro-Generator

In this section we study power management units to supply next-generation ultra-low-power microcontrollers from future micro-generators for applications such as wireless sensor networks or the Internet of Things.

Such applications require energy autonomous operation to avoid battery replacement and the microcontroller must therefore consume the lowest power possible at moderate computing power. For these reasons such future microcontrollers will be supplied at ultra-low voltage (0.3-0.5V) [40]. There is thus a need for dedicated power management units to generate such ultra-low voltages with good conversion efficiency and voltage regulation. Furthermore, these power management units must use as few external components as possible in order to reduce the system volume, the carbon footprint for its production [41] and the assembly costs.

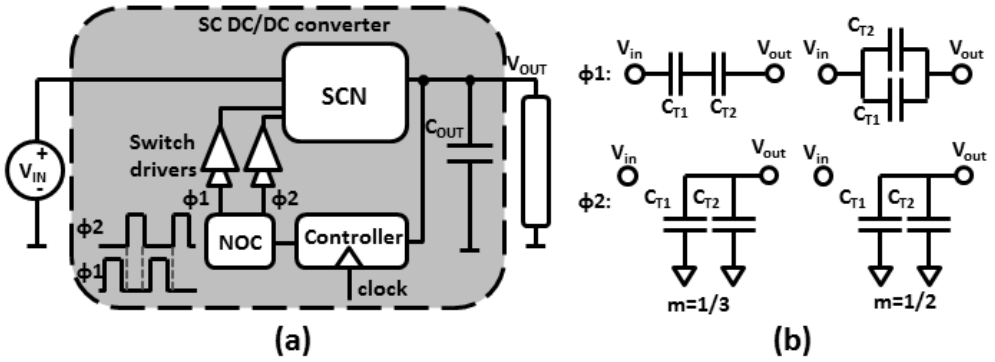

Fig. 12. (a) Architecture of an SC DC/DC converter, (b) Examples of switched-capacitor network with V_{out}/V_{in} conversion ratios of 1/3 and 1/2 at no load.

There are two main families of circuits able to deliver this ultra-low voltage. Firstly, linear regulators dissipate energy in a passive component such as a resistor. Unfortunately the conversion efficiency is limited to the ratio between output and input voltage V_{out}/V_{in}. Secondly, switching converters use switches and inductors or capacitors to convert an input voltage to an output voltage. Inductive switching converters are well known but cannot easily be integrated on-chip and lack efficiency when supplying a low-power load [42]. Switched-capacitor (SC) DC/DC converters can be fully integrated on-chip thanks to the process features of mixed-signal CMOS technologies, and their efficiency remains high at low loads [43], [44]. Fig. 12 (a) shows a typical architecture of such a converter. A switched-capacitor network (SCN) performs the voltage conversion between input and output voltages by oscillating between two phases Φ1 and Φ2. Regulation of the output voltage is performed thanks to a controller that senses V_{out}. Control signals for the actuation of power switches are sent to a block generating non-overlapping clocks (NOC) which ensures that the switches that are ON during the first phase Φ1 are never activated at the same time as the switches that are ON during the second phase Φ2 which would result in unwanted short circuit currents. Gate drivers distribute the control signals from the NOC to the gate of the large power switches while keeping short rise and fall times. Finally an optional output filtering capacitor C_{out} reduces the voltage ripple on V_{out} due to the SCN switching. Fig. 12.(b) shows two examples of SCN with a V_{out}/V_{in} conversion ratio of 1/3 and 1/2 at no load. This ratio can be obtained by inspection of the SCN configurations during the two phases Φ1 and Φ2 of the switching cycle. The power P_{out} that is delivered by such converters to the load is:

$$P_{out} = \alpha f_{sw} (V_{nl} - V_{out}) V_{out}, \quad \text{(Eq.1)}$$

where α depends on the SCN topology, f_{sw} is the converter switching frequency, and V_{nl} is the converter output voltage at no load.

Ultra-low-voltage (ULV) digital circuits such as microcontrollers suffer from high sensitivity to process, voltage and temperature (PVT) variations [45]. Therefore they require a large voltage guard band on their supply voltage to ensure that no timing error occurs in the circuit critical paths in the

worst-case PVT corner, which increases their power consumption. An adaptive voltage scaling (AVS) system using an SC DC/DC converter can be used to (i) provide efficiently the ultra-low voltage for the digital circuit, while (ii) being fully integrated on chip next to the load and while (iii) cancelling the voltage guardband due to PVT variations [45]. Instead of delivering a constant V_{DD} to the circuit, the AVS adapts V_{DD} to ensure that the critical path delay is just below the cycle time of the microcontroller clock (f_{CLK}). The AVS thus compensates the actual PVT corner and avoids the V_{DD} guardband for worst-case PVT variation. The architecture of such an AVS system is shown in Fig. 13. An SC DC/DC converter is used for the voltage conversion. The other blocks of the AVS system are fully digital. A PVT sensor made of a replica of the microcontroller critical path senses its maximal operating frequency under the actual PVT corner. It is also used to provide its clock signal to the load. The external inputs to the AVS system are the battery voltage (V_{BAT}), the value of the microcontroller target frequency (f_{TARGET}) as a digital code and an external low-frequency crystal clock as a reference.

During the high phase of the crystal clock, the frequency comparator counts the number of rising edges of the clock generated by the sensor and clock generation unit. On the falling edge of the crystal clock, the difference between the count result and f_{TARGET} is sent to the regulator. It decides if the circuit clock frequency f_{CLK} must be increased or decreased, to regulate the converter output voltage. It generates control signals which are sent to the decoder that converts them into signals compatible with the DC/DC converter driver. As stated in Eq. (1) the conversion ratio of SC DC/DC converters for a fixed P_{out} depends on the converter switching frequency. For a given P_{out}, the supplied voltage can thus be tuned by controlling the switching frequency of the SC DC/DC converter. The decoder signals control the block generating the converter clock to select its switching frequency. The converter output voltage supplies both the microcontroller and the PVT sensor and clock generation block. When V_{DD} varies, f_{CLK} is automatically adjusted, as the critical path replica ring oscillator frequency is dependent of its supply voltage.

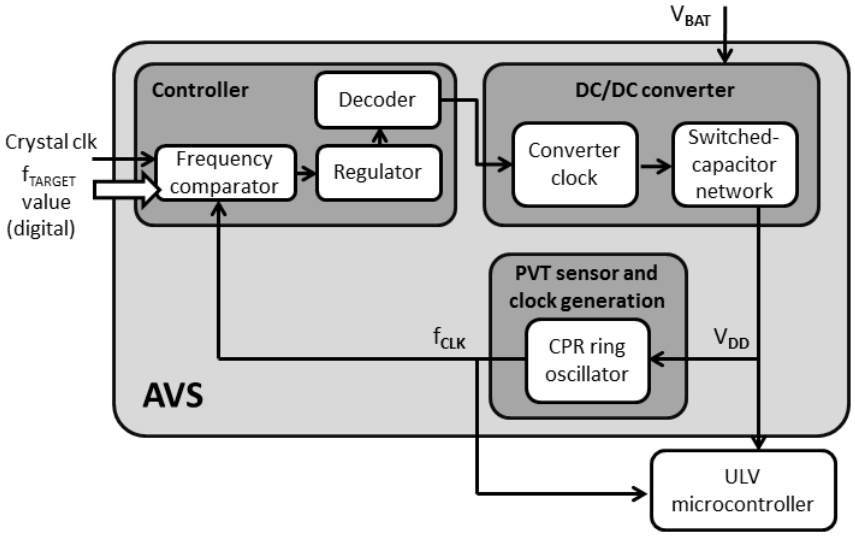

Fig. 13. Block diagram of the proposed adaptive voltage scaling system from [45]. An SC DC/DC converter is used for the voltage conversion, the PVT sensor and clock generation block is built with the same critical-path replica (CPR) ring oscillator.

Fig. 14. shows the transient behavior of such an AVS systems designed to supply the 0.4V SleepWalker microcontroller SoC described in [40]. The start-up procedure is first illustrated: the microcontroller is in sleep mode (V_{DD}=0V with inactive DC/DC converter) and a wake-up request occurs. The clock of the DC/DC converter starts and it sends charges to a 3.3 nF C_{out}.

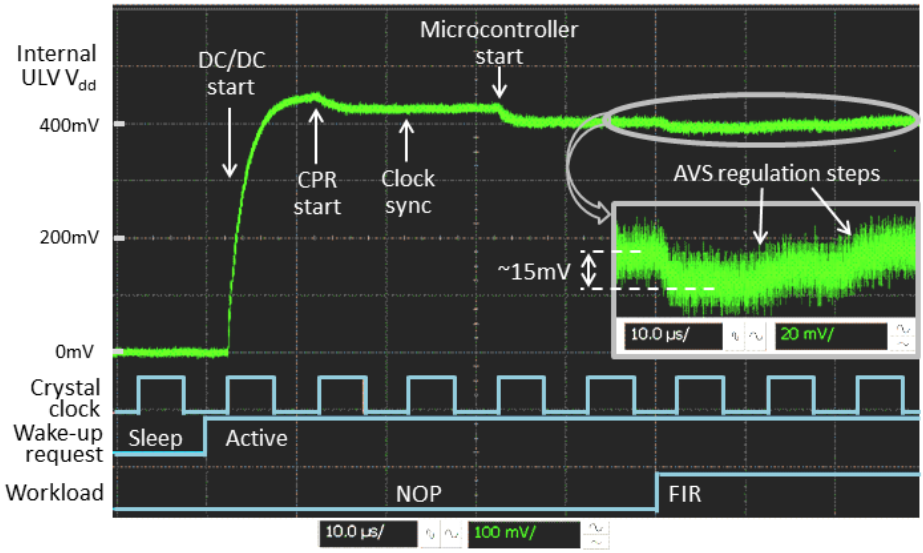

Fig. 14. Measured transient behavior of the voltage supplied by the adaptive voltage scaling systems used in [40] at start-up and for a steep workload change: the microcontroller goes from performing NOP operations to FIR looping.

At this stage, the current consumption of the ULV microcontroller is limited to leakage through the devices. Therefore the AVS output voltage (internal V_{DD}) rises close to the no-load voltage of the SC DC/DC converter, i.e. 500mV. After one period of the crystal clock, the CPR ring oscillator is started and switching power is consumed, resulting in a small drop of the internal V_{DD}. The generated clock is then synchronized with the crystal clock and the operation of the microcontroller is finally started. The AVS loop starts regulating the microcontroller frequency at this stage. Fig. 14 also shows the AVS loop response to a steep workload increase from NOP operations to FIR looping. When the workload changes, the internal V_{DD} only falls by 15mV before going back to target 0.4V.

11.3. Sub-mW Energy Storage Solutions

There is currently a concerted international research effort to bridge the gap between energy demand and supply to enable truly autonomous wireless devices. This requires an increase in both the storage capacity of batteries and the efficiency of energy harvesting devices coupled with a decreased demand from the electronics. Ideally this would be manifest as device integrated energy storage that interfaces with energy harvesting components, provides power on demand to the electronic sensing, communication and display components and operates over the anticipated device lifetime. Ultimately the energy storage solution should occupy a footprint on chip no larger than the electronics it drives, with 1 mm^2 as an attractive long term target for both. No such energy storage component exists today. Batteries are the most common energy storage option & since their introduction in the 1990's lithium ion batteries have exhibited the highest energy density which has been gradually improved in the intervening period from ~200 Wh/l to ~700 Wh/l through the use of improved materials & processing.

Solid state microbatteries which can be processed on Si have achieved similar volumetric energy densities with µm scale thin film materials in large area format, offering capacity retention over thousands of cycles [46]. In the 2D, thin-film geometry, current deposition techniques and lithium ion diffusion limits the electrode thickness to several micrometers resulting in a battery dominated by the substrate and other inactive cell components. As thin films these 2D formats typically exhibit energy densities of ~60 µWh/mm^2 or 0.02 J/mm^2. An energy budget of 1 mWh/day can support a wireless sensor node (WSN) used in building energy management with sensing and transmission every 20 minutes [47]. Clearly significant advances are required for energy storage devices to meet the demand in a reasonable footprint. The key challenges are to realise improved energy storage in a significantly

decreased footprint for Si integration and high rate (power) capability during device interrogation and to decrease recharge time. These challenges require:

- Higher energy density materials, particularly at the cathode, where the current material, LiCoO2, is 25 times less energy dense than lithium metal.
- 3D or 1D active materials structuring with increased aspect ratio providing additional material (stored energy) with respect to planar commercial thin film microbatteries.
- Nanoscale active materials with improved electronic conductivity or core/shell structures [48] to facilitate high rate solid state lithium ion transport.

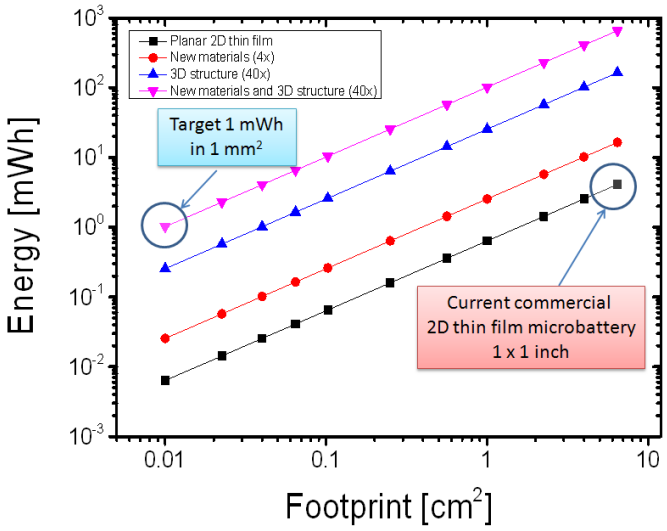

Fig. 15. A roadmap for microbattery energy storage requiring the development and integration of new materials which could yield up to 4 times improvement in stored energy and micro or nanoarchitectures to increase the material quantity and surface area to deliver 1 mWh of energy in a 1 mm^2 footprint.

The need for more energy dense materials and structured electrodes is illustrated in Fig. 15. where the target 1 mWh of energy required for a building management WSN currently has a 6.5 cm^2 footprint. In addition, current solid state microbatteries cannot meet the needs of the ICT systems at peak power during measurement and transceiver operation and require a hybrid energy source. This is due to the lithium diffusion limitation in the solid state electrolyte and cathode. On the other hand the solid state construction does facilitate the use of lithium metal anodes which have a large energy capacity by comparison with the typical carbon anodes (372 mAh/g) of most lithium ion batteries. If non solid state electrolytes are to be utilised then alternative high energy intercalation anodes such as Sn [49] (990 mAh/g), Ge [50] (1,600 mAh/g) or Si [51] (4,200 mAh/g) will be required to prevent dendritic short circuits on cycling. Core/shell [52] versions of these anodes may be required to alleviate mechanical stresses leading to poor cycling behaviour and improve the electronic conductivity to access all of the high aspect ratio structures.

In the Nanofunction project nanoscale materials have been investigated as a means to improve the energy storage and current delivery issues for both anodes and cathodes. Previous research had investigated Cu_6Sn_5 nanowires [53] (Theoretical capacity 605 mAh/g) as potential anodes for a lithium ion microbattery. In this work a Sn rich alloy (Theoretical capacity 830 mAh/g) was investigated to improve the capacity while still delivering an anode that can be structured on Si substrates in nanowire format and permit the use of polymer gel electrolytes to increase rate capability. The $CuSn_3$ nanowires achieved are shown below and representative voltammograms for approximately 6 µm long and 200 nm diameter nanowires are shown in Fig. 16. (a). Initial capacities of 740 mAh/g were recorded for the nanowires with a slow decrease on cycling as seen in Fig 16.(b). The lithium insertion (5 mA) and removal (3 mA) currents for these nanowires also indicate high rate capability.

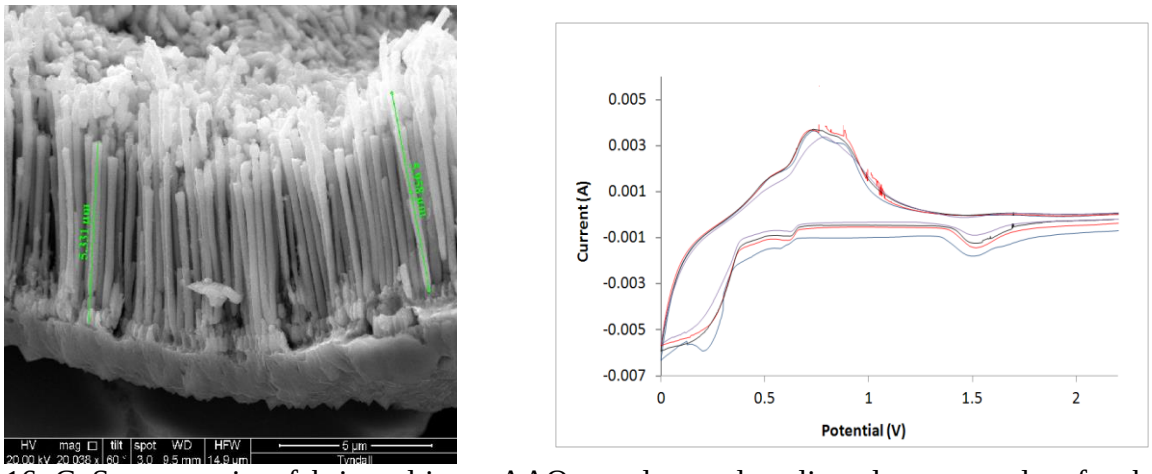

Fig. 16. $CuSn_3$ nanowires fabricated in an AAO template and cyclic voltammetry data for the nanowires.

MnO_2 as an alternative battery cathode to the standard $LiCoO_2$ material is desirable to eliminate the use of the more toxic heavy metal Co of the standard lithium battery and to decrease cost. To integrate the MnO_2 as a battery material required the use of Cu nanotube base supports, also formed in AAO by a method described previously [54] onto which the MnO_2 was deposited. This led to aligned MnO_2 nanowires anchored in the Cu supports as shown in figure 17 forming a well adhered interface. The nanowires are 18 μm long and this aspect ratio of 90 (for 100 nm radius nanowires) results in an active surface area more than 100 times that of the planar footprint. The data for the 18 μm MnO_2 nanowires on Cu supports is shown in figure 17. In the first cycle for the nanowires an improvement is observed for the peak position and rate capability of the lithium insertion and extraction with respect to micron scale MnO_2 material. The influence of the copper support is seen, however, at the more positive potentials and the electrode did not function as expected after the imposition of a high positive potential. Support materials more stable at the high positive potential are required.

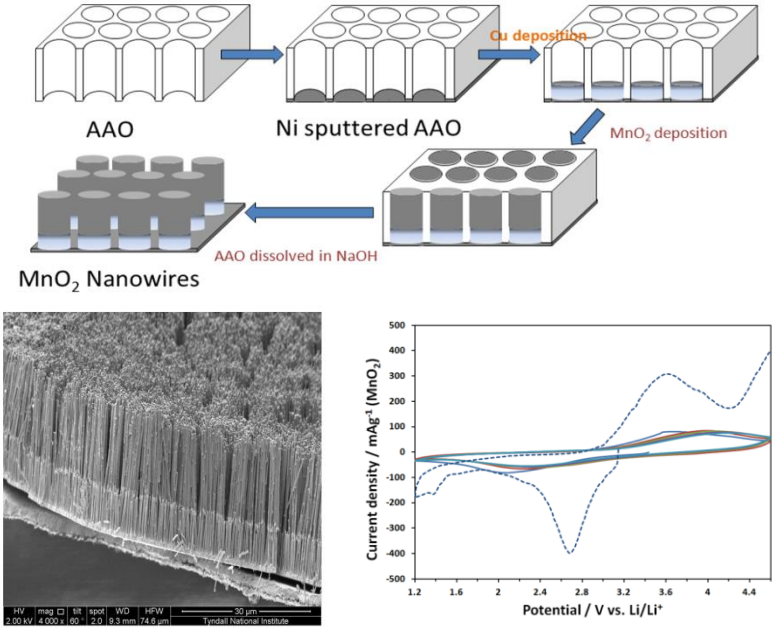

Fig. 17. a) MnO_2 nanowire fabrication route and b) adhered nanowires on Cu nanosupport. c) Li insertion and removal from MnO_2. The solid curves are cycles for <5 μm MnO_2 particles (Aldrich) dispersed on carbon. The dashed line is for the MnO_2 nanowires anchored on Cu.

Despite the gradual improvement there is still a large gap between the energy density of typical cathodes in lithium ion batteries and those of lithium metal or alternative high energy anodes. Disruptive battery technologies such as a Li/sulphur or Li/air [55], [56] can achieve the energy storage requirements of the ICT community. A theoretical energy density of 2.8 mWh/mm^3 (10 J/mm^3) has been estimated for a Li-air battery [57] with non-aqueous electrolytes. It is recognised that the Li/air and other high energy systems have to overcome many obstacles before they will be in widespread deployment but many researchers predict that this could be over the next ten to fifteen years. A very challenging scaling requirement has been shown in Fig.15 and that must be coupled with decreased power requirements in the ultimate device. An increasing focus on improved nanoarchitectures, electrode materials and integrated current collectors is required to surmount these obstacles and deliver high energy density solutions to meet the needs of the electronics industry.

11.4 Conclusions

This chapter introduced power management circuits and energy storage unit designs for sub-1mW low power energy harvesting technologies. This work has proposed three different types of power management circuits for the most frequently used energy harvesting technologies: thermo-electric, photovoltaic and vibrational energy harvesters. The solutions address several of the problems associated with energy harvesting, power management and storage issues including low voltage operation, self-start, efficiency (conversion efficiency as well as impact of power consumption of the power management circuit itself), energy density and leakage current levels. Additionally efforts to miniaturize and integrate magnetics parts as well as integrate discrete circuits onto silicon are outlined to offer improvements in cost, size and efficiency. Finally initial results from efforts to improve energy density of storage devices using nanomaterials are introduced.

For thermo-electric energy harvesting, a transformer based ultra-low voltage ultra-low power (sub-1mW) DC-DC conversion circuit has been proposed. It adopts a novel bonding-wire transformers structure with several types of ferrite/metal material. The bonding wire transformer has been successfully developed in this project for system miniaturization. The implemented transformer obtains a turn ratio up to 1:38. In addition to the PCB implementation of the converter, this technique is also proposed to be utilized in standard CMOS process.

Ultra-low power maximum power point tracking has been developed in this project for sub-1mW indoor solar cells. The fractional open circuit voltage method is proposed in this work for its simple and low power control circuits. The implementation of this MMPT method utilizes nanowatt level comparator logics instead of complicated DSP logics in order to further reduce the power consumption of the MPPT. Power loss simulation model is created to optimize the component selections. The module consumes less than 50μW when the input power is less than 1mW, whilst the end-to-end conversion efficiency of the MPPT circuit is >79.6% with 0.5mW input power.

For vibration energy harvester, a “nano-power” IC has been designed in a 0.32μm STMicroelectronics BCD technology that can manage up to 5 AC-DC channels (e.g. piezoelectric transducers). The IC implements a boost converter based on synchronous electrical charge extraction and be able to convert a wide range of input voltage. For input voltage of 2.5V, the peak efficiency of 85% is achieved in the AC-DC conversion.

An ultra-low supply voltage (<0.5V) micro-controller has been designed in the framework of this project. A DC-DC converter for the future ultra-low voltage microcontroller has been developed in this application. This DC-DC converter steps down the 1.2V energy harvested power to 0.4V supply voltage. The converter is manufactured using 65nm standard CMOS process along with the microcontroller. The maximum conversion efficiency in room temperature is approximately 80%.

In terms of energy storage nanoscale materials have been investigated as a means to improve the storage density and current delivery issues for both anodes and cathodes. Initial capacities of 740 mAh/g were

recorded for the nanowires with a slow decrease on cycling. The lithium insertion (5 mA) and removal (3 mA) currents for these nanowires also indicate high rate capability. Nanowires 18 μm long were developed with an aspect ratio of 90 (for 100 nm radius nanowires) providing an active surface area more than 100 times that of the planar footprint.

Finally these efforts have highlighted the importance of system level methodologies in optimising the overall integrated solution rather than optimising sub-elements in isolation. The benefits of collaboration in Nanofunction have also been clearly illustrated in terms of collaborative testing, specification definition, combining expertise in fabricating miniaturised parts and the synergising of circuit elements from various project partners into next generation high miniaturised efficiency, low leakage multi-source energy harvesting and power management solutions.

References:

[1] Krikke, J. 2005. Sunrise for energy harvesting products. IEEE Pervasive Computing. 4, 1, 4-5.
[2] Energy Conservation Management Inc, 2006. Green and Competitive- The Energy, Environmental, and Economic Benefits of Fiber Glass and Mineral Wool Insulation Products. Web. <http://www.naima.org/pages/resources/library/html>
[3] King, A.W., Dilling, L., Zimmerman, G.P., Fairman, D.M., Houghton, R.A. et al. 2007. North American Carbon Budget and Implications for Global Carbon Cycle. United States DoC Online Library. Web. < www.climatescience.gov/Library/sap/>
[4] Grigg, P. and Slater, A. 2004. Assessment of Energy Efficiency Impact of Building Regulations Compliance Report. Building Research Establishment. Web. <http://www.eeph.org.uk/uploads/documents/partnership/>
[5] Menzel, K., Pesch, D., O'Flynn, B., Keane, M. and O'Mathuna, C. 2008. Towards a Wireless Sensor Platform for Energy Efficient Building Operation. Journal of Tsinghua Science and Technology. 13, S1, 381-386.
[6] Barton, J., O'Flynn, B., Bellis, S., Lynch, A., Morris, M., and O'Mathuna, S.C. 2005. A miniaturised modular platform for wireless sensor networks. In Proceedings of European Conference on Circuit Theory and Design. 3, 35-38.
[7] Doyle, M., Fuller, T. F., and Newman, J. 1993. Modeling of Galvanostatic Charge and Discharge of the Lithium Polymer Insertion Cell. Journal of the Electrochemical Society. 6, 1526-1533.
[8] Hayes, M., Wang, W.S., O'Donnell, T., O'Flynn, B. and O'Mathuna, S.C. 2009. Energy Harvesting for Practical Deployment of Wireless Sensor Networks in Building Energy Management (BEM) Applications. In Proceedings of NanoPower Forum, 102-105.
[9] Randall, J. F. 2005. Designing Indoor Solar Products: Photovoltaic Technologies for AES. John Wiley & Sons.
[10] Doms, I., Merken, P., Mertens and R., Van Hoof, C. 2009. Integrated capacitive power-management circuit for thermal harvesters with output power 10 to 1000uW. In Proceedings of IEEE International Conference on Solid-State Circuits. 300-301.
[11] Roundy, S., Leland, E. S., Baker, J., Carleton, E., Reilly, E. et al. 2005. Improving power output for vibration-based energy scavengers. IEEE Pervasive Computing. 4,1, 28-36.
[12] Shenck, N. S. and Paradiso, J. A. 2001. Energy Scavenging with Shoe-Mounted Piezoelectrics. IEEE Computer Society Journal of Micro. 21, 3, 30-42.
[13] Pereyma, M. 2007. Overview of the Modern State of the Vibration Energy Harvesting Devices. In Proceedings of International Conference on Perspective Technologies and Methods in MEMS Design. 107-112.
[14] Roundy, S. Wright, P.K and Rabaey, J. M. 2003. Energy Scavenging for Wireless Sensor Networks: With Special Focus on Vibrations. Kluwer Academic Publishers.
[15] D. M. Rowe, CRC Handbook of Thermoelectric, ISBN 978-0-8493-0146-9, CRC Press, 1995.
[16] H. Bottner and J. Nurnus, "New high density micro structured thermogenerators for stand alone sensor systems," Thermoelectrics, 2007. ICT 2007. 26th International Conference on, pp. 306–309, 2007.
[17] Po-Hung Chen; Ishida, K.; Xin Zhang; Okuma, Y.; Ryu, Y.; Takamiya, M.; Sakurai, T., "0.18-V input charge pump with forward body biasing in startup circuit using 65nm CMOS," Custom Integrated Circuits Conference (CICC), 2010 IEEE , vol., no., pp.1,4, 19-22 Sept. 2010.
[18] Po-Hung Chen, K. Ishida, ; Ikeuchi, K.; Xin Zhang; Honda, K.; Okuma, Y.; Ryu, Y.; Takamiya, M.; Sakurai, T., "Startup Techniques for 95 mV Step-Up Converter by Capacitor Pass-On Scheme and VTH-Tuned Oscillator With Fixed Charge Programming," Solid-State Circuits, IEEE Journal of , vol.47, no.5, pp.1252,1260, May 2012.
[19] Ramadass, Y.K.; Chandrakasan, A.P., "A Battery-Less Thermoelectric Energy Harvesting Interface Circuit With 35 mV Startup Voltage," Solid-State Circuits, IEEE Journal of , vol.46, no.1, pp.333,341, Jan. 2011.
[20] Damaschke, J.M., "Design of a low-input-voltage converter for thermoelectric generator," Industry Applications, IEEE Transactions on , vol.33, no.5, pp.1203,1207, Sep/Oct 1997.
[21] Linear Technology, "LTC3108. Ultralow Voltage Step-Up Converter and Power Manager", device data sheet
[22] Jong-Pil Im; Se-Won Wang; Seung-Tak Ryu; Gyu-Hyeong Cho, "A 40 mV Transformer-Reuse Self-Startup Boost Converter With MPPT Control for Thermoelectric Energy Harvesting," Solid-State Circuits, IEEE Journal of , vol.47, no.12, pp.3055,3067, Dec. 2012.
[23] Lu, J. et al. "Modelling, design and characterization of multiturn bondwire inductors with ferrite epoxy glob cores for power supply system-on-chip or system in package applications," IEEE TPE Aug. 2010.
[24] Mathúna, C.O.; Ningning Wang; Kulkarni, S.; Roy, S.; , "Review of Integrated Magnetics for Power Supply on Chip (PwrSoC)," Power Electronics, IEEE Transactions on , vol.27, no.11, pp.4799-4816, Nov. 2012.
[25] Koutroulis, E.; Kalaitzakis, K.; Voulgaris, N.C.; , "Development of a microcontroller-based, photovoltaic maximum power point tracking control system," Power Electronics, IEEE Transactions on , vol.16, no.1, pp.46-54, Jan 2001
[26] Simjee, F.I.; Chou, P.H.; , "Efficient Charging of Supercapacitors for Extended Lifetime of Wireless Sensor Nodes," Power Electronics, IEEE Transactions on , vol.23, no.3, pp.1526-1536, May 2008

[27] Dondi, D.; Bertacchini, A.; Brunelli, D.; Larcher, L.; Benini, L.; , "Modeling and Optimization of a Solar Energy Harvester System for Self-Powered Wireless Sensor Networks," Industrial Electronics, IEEE Transactions on , vol.55, no.7, pp.2759-2766, July 2008
[28] Brunelli, D.; Moser, C.; Thiele, L.; Benini, L.; , "Design of a Solar-Harvesting Circuit for Batteryless Embedded Systems," Circuits and Systems I: Regular Papers, IEEE Transactions on , vol.56, no.11, pp.2519-2528, Nov. 2009
[29] Brunelli, D.; Benini, L.; , "Designing and managing sub-milliwatt energy harvesting nodes: Opportunities and challenges," Wireless Communication, Vehicular Technology, Information Theory and Aerospace & Electronic Systems Technology, 2009. Wireless VITAE 2009. 1st International Conference on , vol., no., pp.11-15, 17-20 May 2009
[30] Yen Kheng Tan; Panda, S.K.; , "Optimized Wind Energy Harvesting System Using Resistance Emulator and Active Rectifier for Wireless Sensor Nodes," Power Electronics, IEEE Transactions on , vol.26, no.1, pp.38-50, Jan. 2011
[31] Chini, A.; Rovati, L.; , "Micro-power photovoltaic harvester based on a frequency-to-voltage MPPT tracker," Electronics Letters , vol.46, no.8, pp.587-589, April 15 2010
[32] Simjee, F.; Chou, P.H.; , "Everlast: Long-life, Supercapacitor-operated Wireless Sensor Node," Low Power Electronics and Design, 2006. ISLPED'06. Proceedings of the 2006 International Symposium on , pp.197-202, 4-6 Oct. 2006
[33] S. Roundy, et al., "A study of low level vibrations as a power source for wireless sensor nodes," Computer Communications, vol. 26, no. 11, pp. 1131-1144, Jul. 2003
[34] Romani, A., et al. "Actively controlled power conversion techniques for piezoelectric energy harvesting applications." Sensors and Microsystems. Springer Netherlands, 2010. 359-363.
[35] E. Lefeuvre, A. Badel, C. Richard, L. Petit, D. Guyomar, A comparison between several vibration-powered piezoelectric generators for standalone systems, Sensors and Actuators A: Physical, Volume 126, Issue 2, 14 February 2006, Pages 405-416
[36] A. Romani, C. Tamburini, R. P. Paganelli, A. Golfarelli, R. Codeluppi, E. Sangiorgi, M. Tartagni, "Dynamic Switching Conversion for Piezoelectric Energy Harvesting Systems", IEEE Sensors 2008, pp. 689-692
[37] Dallago, E.; Miatton, D.; Venchi, G.; Bottarel, V.; Frattini, G.; Ricotti, G.; Schipani, M., "Electronic interface for Piezoelectric Energy Scavenging System," Solid-State Circuits Conference, 2008. ESSCIRC 2008. 34th European , vol., no., pp.402,405, 15-19 Sept. 2008
[38] A. Romani, et al., "A Scalable Micro-power Converter for Multi-source Piezoelectric Energy Harvesting Applications," Procedia Engineering, vol. 5, no. 2009, pp. 782-785, 2010
[39] M. Dini, et al. "A nano-power energy harvesting IC for arrays of piezoelectric transducers." SPIE Microtechnologies. International Society for Optics and Photonics, 2013
[40] D. Bol et al, "SleepWalker: A 25-MHz 0.4-V Sub-mm2 7-µW/MHz Microcontroller in 65-nm LP/GP CMOS for Low-Carbon Wireless Sensor Nodes", in IEEE J. Solid- State Circuits, vol. 48 (1), pp. 20-32, 2013.
[41] D. Bol, et al,, "Green SoCs for a sustainable Internet-of-Things," in in Proc. IEEE Low-Voltage Low-Power Conf. (FTFC), , pp.1,4, 20-21, 2013.
[42] M. Belleville, et al, "Energy autonomous sensor systems: Towards a ubiquitous sensor technology", in Microelectronics Journal, vol. 41 (11), 2010, pp. 740-745.
[43] G. V. Piqué and H. J. Bergveld, "State-of-the-art of integrated switching power converters", in Analog Circuit Design, Springer Netherlands, pp. 259-281, 2012.
[44] T. Van Breussegem, M. Wens, and M. Steyaert, "Control of Fully Integrated DC-DC Converters in CMOS", in Analog Circuit Design, Springer Netherlands, pp. 259-281, 2012.
[45] J. De Vos, D. Flandre and D. Bol, "Pushing adaptive voltage scaling fully on chip", in ASP J. Low-Power Electronics, vol. 8, pp. 95-105, 2012.
[46] Dudney, N. J. Mat Sci Eng B-Solid 2005, 116, 245.
[47] O'Mathuna, C. ; O'Donnell, T.; Martinez-Catala, R. V.; Rohan, J.; O'Flynn, B. Talanta 2008, 75, 613.
[48] Hasan, M.; Chowdhury, T.; Rohan, J. F. Journal of the Electrochemical Society 2010, 157, A682.
[49] Whitehead, A. H.; Elliott, J. M.; Owen, J. R. Journal of Power Sources 1999, 81, 33.
[50] Laforge, B.; Levan-Jodin, L.; Salot, R.; Billard, A. Journal of the Electrochemical Society 2008, 155, A181.
[51] Chan, C. K.; Peng, H. L.; Liu, G.; McIlwrath, K.; Zhang, X. F.; Huggins, R. A.; Cui, Y. Nat Nanotechnol 2008, 3, 31.
[52] Cui, L. F.; Ruffo, R.; Chan, C. K.; Peng, H. L.; Cui, Y. Nano Lett 2009, 9, 491.
[53] Rohan, J. F.; Hasan, M.; Holubowitch, N. Electrochimica Acta 2011, 56, 9537.
[54] Chowdhury, T.; Casey, D. P.; Rohan, J. F. Electrochemistry Communications 2009, 11, 1203.
[55] Abraham, K. M.; Jiang, Z. Journal of the Electrochemical Society 1996, 143, 1.
[56] Bruce, P. G.; Hardwick, L. J.; Abraham, K. M. Mrs Bull 2011, 36, 506.
[57] Zheng, J. P.; Liang, R. Y.; Hendrickson, M.; Plichta, E. J. JOURNAL OF THE ELECTROCHEMICAL SOCIETY 2008, 155, A432.